

# A First Measurement of Low $x$ Low $Q^2$ Structure Functions in Neutrino Scattering

B. T. Fleming,<sup>2</sup> T. Adams,<sup>4</sup> A. Alton,<sup>4</sup> C. G. Arroyo,<sup>2</sup> S. Avvakumov,<sup>7</sup> L. de Barbaro,<sup>5</sup> P. de Barbaro,<sup>7</sup>  
 A. O. Bazarko,<sup>2</sup> R. H. Bernstein,<sup>3</sup> A. Bodek,<sup>7</sup> T. Bolton,<sup>4</sup> J. Brau,<sup>6</sup> D. Buchholz,<sup>5</sup> H. Budd,<sup>7</sup> L. Bugel,<sup>3</sup> J. Conrad,<sup>2</sup>  
 R. B. Drucker,<sup>6</sup> J. A. Formaggio,<sup>2</sup> R. Frey,<sup>6</sup> J. Goldman,<sup>4</sup> M. Goncharov,<sup>4</sup> D. A. Harris,<sup>7</sup> R. A. Johnson,<sup>1</sup>  
 J. H. Kim,<sup>2</sup> B. J. King,<sup>2</sup> T. Kinnel,<sup>8</sup> S. Koutsoliotas,<sup>2</sup> M. J. Lamm,<sup>3</sup> W. Marsh,<sup>3</sup> D. Mason,<sup>6</sup> K. S. McFarland,<sup>7</sup>  
 C. McNulty,<sup>2</sup> S. R. Mishra,<sup>2</sup> D. Naples,<sup>4</sup> P. Nienaber,<sup>3</sup> A. Romosan,<sup>2</sup> W. K. Sakumoto,<sup>7</sup> H. Schellman,<sup>5</sup>  
 F. J. Sciulli,<sup>2</sup> W. G. Seligman,<sup>2</sup> M. H. Shaevitz,<sup>2</sup> W. H. Smith,<sup>8</sup> P. Spentzouris,<sup>2</sup> E. G. Stern,<sup>2</sup> N. Suwonjandee,<sup>1</sup>  
 A. Vaitaitis,<sup>2</sup> M. Vakili,<sup>1</sup> U. K. Yang,<sup>7</sup> J. Yu,<sup>3</sup> G. P. Zeller,<sup>5</sup> and E. D. Zimmerman<sup>2</sup>

( *The CCFR/NuTeV Collaboration* )

<sup>1</sup> *University of Cincinnati, Cincinnati, OH 45221*

<sup>2</sup> *Columbia University, New York, NY 10027*

<sup>3</sup> *Fermi National Accelerator Laboratory, Batavia, IL 60510*

<sup>4</sup> *Kansas State University, Manhattan, KS 66506*

<sup>5</sup> *Northwestern University, Evanston, IL 60208*

<sup>6</sup> *University of Oregon, Eugene, OR 97403*

<sup>7</sup> *University of Rochester, Rochester, NY 14627*

<sup>8</sup> *University of Wisconsin, Madison, WI 53706*

A new structure function analysis of CCFR deep inelastic  $\nu$ -N and  $\bar{\nu}$ -N scattering data is presented for previously unexplored kinematic regions down to Bjorken  $x = 0.0045$  and  $Q^2 = 0.3 \text{ GeV}^2$ . Comparisons to charged lepton scattering data from NMC [1] and E665 [2] experiments are made and the behavior of the structure function  $F_2^\nu$  is studied in the limit  $Q^2 \rightarrow 0$ .

Neutrino structure function measurements in the low Bjorken  $x$ , low  $Q^2$  region can be used to study the axial-vector component of the weak interaction as well as to test the limits of parton distribution universality. In this paper, we present a first measurement of the structure function  $F_2$  in neutrino scattering, from the CCFR data, for  $Q^2 < 1 \text{ GeV}^2$  and  $0.0045 < x < 0.035$ . In this region where perturbative and non-perturbative QCD meet, we present a parameterization of the data which allows us to test the partially conserved axial current (PCAC) limit of  $F_2$  in neutrino scattering.

The universality of parton distributions can be tested by comparing neutrino scattering data to charged lepton scattering data. Past measurements for  $0.0075 < x < 0.1$  and  $Q^2 > 1.0 \text{ GeV}^2$  have indicated that  $F_2^\nu$  differs from  $F_2^\mu$  by 10-15% [3]. This discrepancy has been partially resolved by recent analyses of  $F_2^\nu$  at  $Q^2 > 1.0 \text{ GeV}^2$  [4,5]. While we expect and have now observed that parton distribution universality holds in this region, this need not be the case at lower values of  $Q^2$ . Deviations from this universality at lower  $Q^2$  are expected due to differences in vector and axial components of electromagnetic and weak interactions. In particular, the electromagnetic interaction has only a vector component while the weak interaction has both vector and axial-vector components. Vector currents are conserved (CVC) but axial-vector currents are only partially conserved (PCAC). Adler [6] proposed a test of the PCAC hypothesis using high energy neutrino interactions, a consequence of which is the prediction that  $F_2$  approaches a non-zero constant as  $Q^2 \rightarrow 0$  due to U(1) gauge invariance. A determination of this constant is performed here by fitting the low  $Q^2$  data to a phenomenological curve developed by Donnachie and Landshoff [7].

The differential cross-sections for the  $\nu N$  charged-current process  $\nu_\mu (\bar{\nu}_\mu) + N \rightarrow \mu^- (\mu^+) + X$  in the limit of negligible quark masses and neglecting lepton masses, in terms of the Lorentz-invariant structure functions  $F_2$ ,  $2xF_1$ , and  $xF_3$  are:

$$\frac{d\sigma^{\nu,\bar{\nu}}}{dx dy} = \frac{G_F^2 M E_\nu}{\pi} \left[ \left( 1 - y - \frac{Mxy}{2E_\nu} \right) F_2(x, Q^2) + \frac{y^2}{2} 2xF_1(x, Q^2) \pm y \left( 1 - \frac{y}{2} \right) xF_3(x, Q^2) \right] \quad (1)$$

where  $G_F$  is the weak Fermi coupling constant,  $M$  is the nucleon mass,  $E_\nu$  is the incident  $\nu$  energy,  $Q^2$  is the square of the four-momentum transfer to the nucleon, the scaling variable  $y = E_{HAD}/E_\nu$  is the fractional energy transferred to the hadronic vertex with  $E_{HAD}$  equal to the measured hadronic energy, and  $x = Q^2/2ME_\nu y$ , the Bjorken scaling variable, is the fractional momentum carried by the struck quark. The structure function  $2xF_1$  is expressed in terms of  $F_2$  by  $2xF_1(x, Q^2) = F_2(x, Q^2) \times \frac{1+4M^2x^2/Q^2}{1+R(x, Q^2)}$ , where  $R = \frac{\sigma_L}{\sigma_T}$  is the ratio of the cross-sections of longitudinally to transversely-

polarized  $W$  bosons. In the leading order (LO) quark-parton model,  $F_2$  is the sum of the momentum densities of all interacting quark constituents, and  $xF_3$  is the difference of these, the valence quark momentum density; these relations are modified by higher-order QCD corrections.

The  $\nu$  deep inelastic scattering (DIS) data were collected in two high-energy high-statistics runs, FNAL E744 and E770, in the Fermilab Tevatron fixed-target quadrupole triplet beam (QTB) line by the CCFR collaboration. The detector [8,9] consists of a target calorimeter instrumented with both scintillators and drift chambers for measuring the energy of the hadron shower,  $E_{HAD}$ , and the muon angle,  $\theta_\mu$ , followed by a toroid spectrometer for measuring the muon momentum  $p_\mu$ . There are 1,030,000  $\nu_\mu$  events and 179,000  $\bar{\nu}_\mu$  events in the data sample after fiducial volume and geometric cuts, and kinematic cuts of  $p_\mu > 15 \text{ GeV}$ ,  $\theta_\mu < 150 \text{ mr}$ ,  $E_{HAD} > 10 \text{ GeV}$ , and  $30 < E_\nu < 360 \text{ GeV}$ . These cuts were applied to select regions of high efficiency and small systematic errors in reconstruction.

The structure function  $F_2$  in Eq. (1) can be calculated from the observed number of  $\nu_\mu$  and  $\bar{\nu}_\mu$  events combined with the  $\nu_\mu$  and  $\bar{\nu}_\mu$  fluxes. The ratio of fluxes between different energies in  $\nu$  mode and that between  $\bar{\nu}$  and  $\nu$  mode was determined using the events with  $E_{HAD} < 20 \text{ GeV}$  [10–12]. The overall normalization of the flux was constrained such that the measured total neutrino-nucleon cross-section for  $\nu s$  equaled the world average cross-section for isoscalar-corrected iron target experiments,  $\sigma^{\nu Fe}/E = (0.677 \pm 0.014) \times 10^{-38} \text{ cm}^2/\text{GeV}$  [11,13] and for  $\bar{\nu}s$  equaled the world average cross-section including this experiment for isoscalar-corrected iron target experiments,  $\sigma^{\bar{\nu} Fe}/E = (0.340 \pm 0.007) \times 10^{-38} \text{ cm}^2/\text{GeV}$ . Negligible corrections for non-isoscalarity of the iron target and the mass of the  $W$  boson propagator are applied.

Sources of systematic error on  $F_2$  arise from limitations of the models used for corrections and from the level of our knowledge of the detector calibration. Muon and hadron energy calibrations were determined from test beam data collected during the course of the experiment [8,9]. For acceptance, smearing, and radiative corrections we chose an appropriate model for the low  $x$ , low  $Q^2$  region, the GRV [14] model of the parton distribution functions. The GRV model is used up to  $Q^2 = 1.35 \text{ GeV}^2$  where it is normalized to a LO parameterization [15] used above this. Inclusion of the GRV model in the radiative correction calculation caused a systematic decrease in  $F_2$  by as much as 10% in the lowest  $x$  bin, decreasing to 1-2% at  $x = 0.015$  as compared to the effects of the LO model used in the previous analysis [10]. Due to the systematic uncertainty in the model at low  $x$ , the radiative correction error is 3% in the lowest  $x$  bin. A correction is applied for the difference between  $xF_3^\nu$  and  $xF_3^{\bar{\nu}}$ , determined using a LO calculation of  $\Delta xF_3 = xF_3^\nu - xF_3^{\bar{\nu}}$ . The recent CCFR  $\Delta xF_3$  measurement [4] is higher than this

LO model [15] and all other current LO and NLO theoretical predictions in this kinematic region. An appropriate systematic error is applied to account for the differences between the theory and this measurement. Finally, a systematic error is applied to account for the uncertainty in the value of  $R$ , which comes from a global fit to the world's measurements [16].

In previous analyses a slow rescaling correction was applied to account for massive charm effects. This is not applied here since the corrections are model dependent and uncertain in this kinematic range. As a result, neutrino and charged lepton DIS data must be compared within the framework of charm production models, accomplished by plotting the ratio of data to theoretical model. The theoretical calculation corresponding to the CCFR data employs NLO QCD including heavy flavor effects as implemented in the TR-VFS(MRST99) scheme [17,18]. The theoretical calculation corresponding to NMC and E665 data is determined using TR-VFS(MRST99) for charged lepton scattering. Other theoretical predictions such as ACOT-VFS(CTEQ4HQ) [19,20] and FFS(GRV94) [21] do not significantly change the comparison.

The combination of the inclusion of the GRV model at low  $x$  and low  $Q^2$ , its effect on the radiative corrections, and removal of the slow rescaling correction help to resolve the longstanding discrepancy between the neutrino and charged lepton DIS data above  $x = 0.015$ .  $F_2$  is plotted in Figure 1. Errors are statistical and systematic added in quadrature. A line is drawn at  $Q^2 = 1 \text{ GeV}^2$  to highlight the kinematic region this analysis accesses. Figure 2 compares  $F_2$  (data/theoretical model) for CCFR, NMC, and E665. There is agreement to within 5% down to  $x = 0.0125$ . Below this, as  $x$  decreases, CCFR  $F_2$  (data/theory) becomes systematically higher than NMC  $F_2$  (data/theory). Differences between scattering via the weak interaction and via the electromagnetic interaction as  $Q^2 \rightarrow 0$  may account for the disagreement in this region.

In charged lepton DIS, the structure function  $F_2$  is constrained by gauge invariance to vanish with  $Q^2$  as  $Q^2 \rightarrow 0$ . Donnachie and Landshoff predict that in the low  $Q^2$  region,  $F_2^\mu$  will follow the form [7]:

$$C \left( \frac{Q^2}{Q^2 + A^2} \right). \quad (2)$$

However, in the case of neutrino DIS, the axial component of the weak interaction may contribute a nonzero component to  $F_2$  as  $Q^2$  approaches zero. Donnachie and Landshoff predict that  $F_2^\nu$  should follow a form with a non-zero contribution at  $Q^2 = 0$ :

$$\frac{C}{2} \left( \frac{Q^2}{Q^2 + A^2} + \frac{Q^2 + D}{Q^2 + B^2} \right). \quad (3)$$

Using NMC and E665 data, corrected in this case to be equivalent to scattering from an iron target using a pa-

rameterization of SLAC Fe/D data [10], we do a combined fit to the form predicted for  $\mu$  DIS and extract the parameter  $A = 0.81 \pm 0.02$  with  $\chi^2/DOF = 27/17$ . Results of fits in each  $x$  bin for each experiment are shown in Table I for comparison to parameters in the CCFR fit. The error on  $A$  is incorporated in the systematic error on the final fit. Inserting this value for  $A$  into the form predicted for  $\nu$ N DIS, we fit CCFR data to extract parameters  $B$ ,  $C$ , and  $D$ , and determine the value of  $F_2$  at  $Q^2 = 0$ . Only data below  $Q^2 = 1.4 \text{ GeV}^2$  are used in the fits. The CCFR  $x$ -bins that contain enough data to produce a good fit in this  $Q^2$  region are  $x = 0.0045$ ,  $x = 0.0080$ ,  $x = 0.0125$ , and  $x = 0.0175$ . Figure 3 and Table II show the results of the fits. Error bars consist of statistical and systematic terms added in quadrature but exclude an overall correlated normalization uncertainty of 1-2%. The values of  $F_2$  at  $Q^2 = 0 \text{ GeV}^2$  in the three highest  $x$ -bins are statistically significant and are within  $1\sigma$  of each other. The lowest  $x$  bin has large error bars but is within  $1.5\sigma$  of the others. Taking a weighted average of the parameters  $B$ ,  $C$ ,  $D$ , and  $F_2$  yields  $B = 1.53 \pm 0.02$ ,  $C = 2.31 \pm 0.03$ ,  $D = 0.48 \pm 0.03$ , and  $F_2(Q^2 = 0) = 0.21 \pm 0.02$ . Figure 4 shows  $F_2(Q^2 = 0)$  for the different  $x$  bins. Inclusion of an  $x$  dependence of the form  $x^\beta$  does not change the overall fits or  $\chi^2$ s. However, unlike in charged lepton scattering, the Donnachie and Landshoff mass parameter,  $B$ , appears to depend on  $x$ , with higher values corresponding to higher  $x$ . Thus,  $F_2$  at higher  $x$  approaches  $F_2(Q^2 = 0)$  more slowly than at lower  $x$ .

In summary, a comparison of  $F_2$  from neutrino DIS to that from charged lepton DIS shows good agreement above  $x = 0.0125$ , but shows differences at smaller  $x$ . This low  $x$  discrepancy can be explained by the different behavior of  $F_2$  from  $\nu$  DIS to that from  $e/\mu$  DIS as  $Q^2 \rightarrow 0$ . CCFR  $F_2^\nu$  data favors a non-zero value for  $F_2$  as  $Q^2 \rightarrow 0$ .

We would like to thank the management and staff of Fermilab, and acknowledge the help of many individuals at our home institutions. We would also like to thank Fred Olness for many useful discussions [22]. This research was supported by the National Science Foundation and the Department of Energy of the United States, who should be credited for their continued support of basic research.

## REFERENCES

- 
- [1] M. Arneodo *et al.*, *Nucl. Phys.* **B483**: 3 (1997).

- [2] M. R. Adams *et al.*, *Phys. Rev.* **D54**: 3006 (1996)
- [3] W. G. Seligman *et al.*, *Phys. Rev. Lett.* **79**: 1213 (1997).
- [4] U. K. Yang *et al.*, UR-1586, submitted to *Phys. Rev. Lett.* (2000).
- [5] C. Boros, F. M. Steffens, J. T. Londergan, A. W. Thomas *Phys. Lett.* **B468**:161-167 (1999)
- [6] S. L. Adler, *Phys. Rev.* **B135**: 963 (1964).
- [7] A. Donnachie and P.V. Landshoff *Z. Phys.* **C61**: 139 (1994).
- [8] W. K. Sakumoto *et al.*, *Nucl. Instrum. Meth.* **A294**: 179 (1990).
- [9] B. J. King *et al.*, *Nucl. Instrum. Meth.* **A302**: 254 (1991).
- [10] W. G. Seligman, Ph.D. Thesis, Nevis Report 292.
- [11] P. S. Auchincloss *et al.*, *Z. Phys.* **C48**: 411 (1990).
- [12] R. Belusevic and D. Rein, *Phys. Rev.* **D38**: 2753 (1988).
- [13] R. Blair *et al.*, *Phys. Rev. Lett.* **51**: 343 (1983); P. Berge *et al.*, *Z. Phys.* **C49**: 187 (1991).
- [14] M. Glück, E. Reya, and A. Vogt, *Z. Phys.* **C67**: 433 (1995)
- [15] A. J. Buras and K. J. F. Gaemers, *Nucl. Phys.* **B132**: 249 (1978).
- [16] L. W. Whitlow *et al.*, *Phys. Lett.* **B250**: 193 (1990).
- [17] R. S. Thorne and R. G. Roberts, *Phys. Lett* **B421**: 303 (1998).
- [18] A.D. Martin *et al.*, *Eur. Phys. J.* **C4**: 463 (1998), (we have used the post DIS-2000 MRST corrected code).
- [19] M. Aivazis, J. Collins, F. Olness, and W. K. Tung, *Phys. Rev.* **D50**: 3102 (1994).
- [20] M. Aivazis, F. Olness, and W. K. Tung, *Phys. Rev. Lett.* **65**: 2339 (1990).
- [21] E. Laenen, S. Riemersma, J. Smith, and W. L. Van Neervan, *Nucl. Phys.* **B392**: 162 (1993).
- [22] F. Olness (private communication).

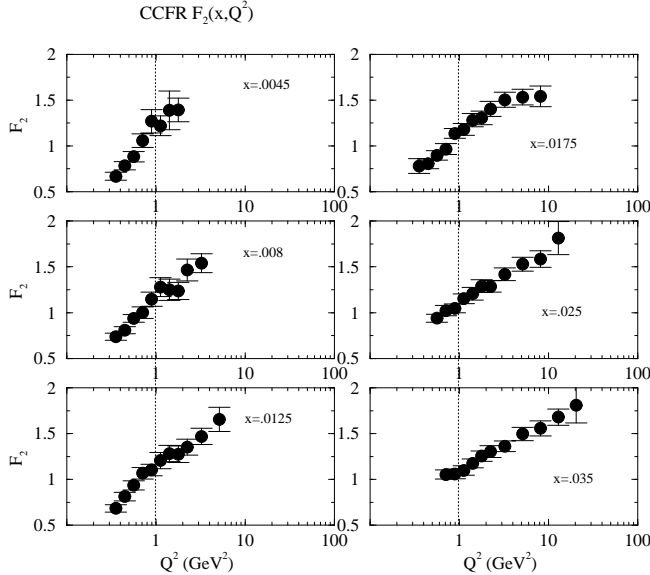


FIG. 1. CCFR  $F_2$  at low  $x$ , low  $Q^2$ . Data to the left of the vertical line at  $Q^2 = 1.0$  represent the new kinematic regime for this analysis.

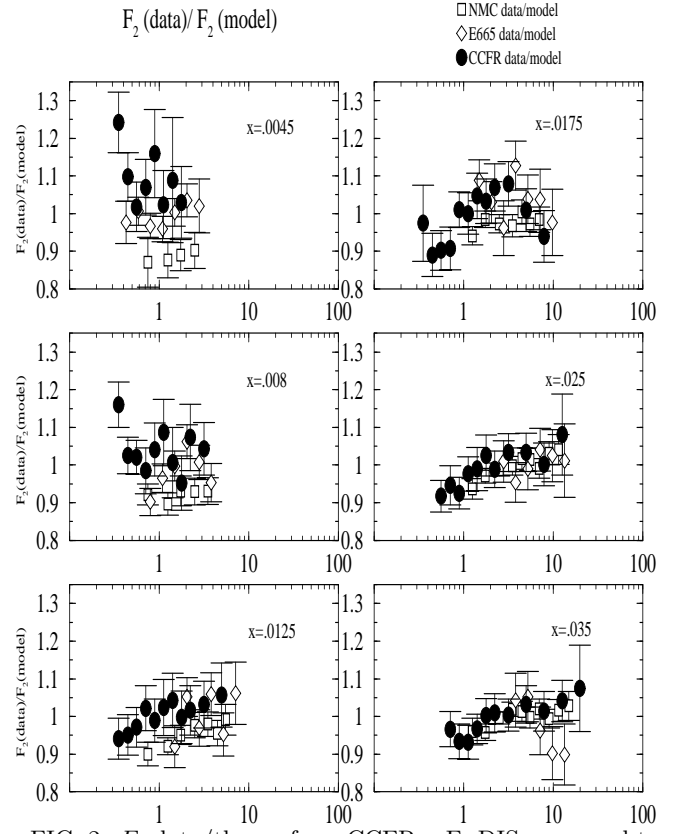


FIG. 2.  $F_2$  data/theory from CCFR  $\nu$ -Fe DIS compared to  $F_2$  from NMC and E665 DIS. Errors bars are statistical and systematic added in quadrature. Theoretical predictions are those of TR-VFS(MRST99).

TABLE I. Results for NMC and E665 data fit to Eq. 2.

$x$	$A$	$\chi^2/N$	$N$
0.0045(NMC)	$0.87 \pm 0.16$	0.02	2
0.0045(E665) <sup>a</sup>	$0.90 \pm 0.10$	0.43	4
0.0045(E665) <sup>b</sup>	$0.94 \pm 0.09$	0.31	5
0.0080(NMC)	$0.75 \pm 0.07$	0.38	3
0.0080(E665) <sup>c</sup>	$0.87 \pm 0.10$	0.24	4
0.0080(E665) <sup>d</sup>	$0.85 \pm 0.11$	1.19	4
0.0125(NMC)	$0.81 \pm 0.05$	0.55	5
0.0125(E665)	$0.97 \pm 0.14$	1.12	4
0.0175(NMC)	$0.78 \pm 0.06$	0.38	5
0.0175(E665)	$0.76 \pm 0.13$	0.88	5

<sup>a</sup>Bin center corrected from  $x = 0.004$

<sup>b</sup>Bin center corrected from  $x = 0.005$

<sup>c</sup>Bin center corrected from  $x = 0.007$

<sup>d</sup>Bin center corrected from  $x = 0.009$

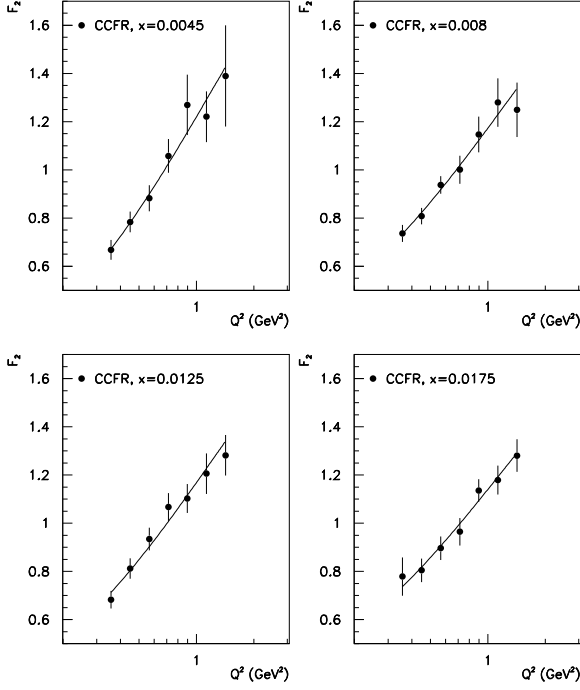


FIG. 3. Results from fit to CCFR data to extrapolate to  $F_2(Q^2 = 0)$ .

TABLE II. Fit results for CCFR data. CCFR data is fit to Eq. 4 with  $A = 0.81 \pm 0.02$  as determined by fits to NMC and E665 data. B, C, D, and  $F_2$  at  $Q^2 = 0$  results shown below.  $N = 4$  for all fits.

$x$	$B$	$C$	$D$	$F_2^\nu(Q^2 = 0)$	$\chi^2/N$
0.0045	$1.49 \pm 0.02$	$2.62 \pm 0.26$	$0.06 \pm 0.17$	$0.04 \pm 0.10$	0.5
0.0080	$1.63 \pm 0.05$	$2.32 \pm 0.05$	$0.50 \pm 0.05$	$0.22 \pm 0.03$	0.5
0.0125	$1.63 \pm 0.05$	$2.39 \pm 0.05$	$0.40 \pm 0.05$	$0.18 \pm 0.03$	1.0
0.0175	$1.67 \pm 0.05$	$2.20 \pm 0.05$	$0.65 \pm 0.07$	$0.26 \pm 0.03$	0.5

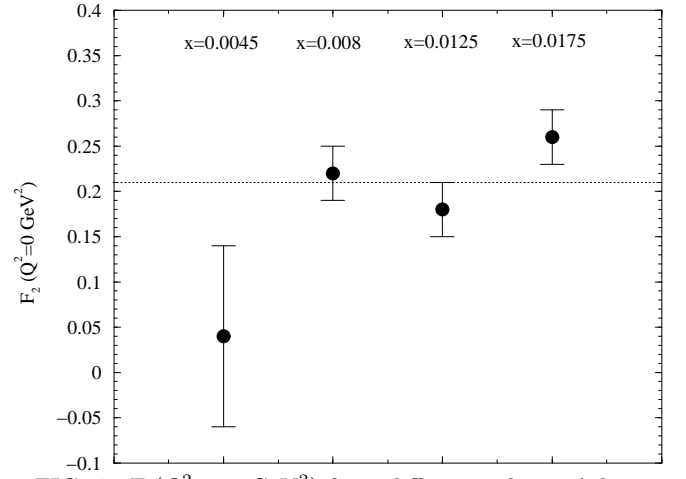


FIG. 4.  $F_2(Q^2 = 0 \text{ GeV}^2)$  from different  $x$  bins. A line is drawn at the weighted average of all four measurements.